

RSC Advances



This is an *Accepted Manuscript*, which has been through the Royal Society of Chemistry peer review process and has been accepted for publication.

Accepted Manuscripts are published online shortly after acceptance, before technical editing, formatting and proof reading. Using this free service, authors can make their results available to the community, in citable form, before we publish the edited article. This *Accepted Manuscript* will be replaced by the edited, formatted and paginated article as soon as this is available.

You can find more information about *Accepted Manuscripts* in the [Information for Authors](#).

Please note that technical editing may introduce minor changes to the text and/or graphics, which may alter content. The journal's standard [Terms & Conditions](#) and the [Ethical guidelines](#) still apply. In no event shall the Royal Society of Chemistry be held responsible for any errors or omissions in this *Accepted Manuscript* or any consequences arising from the use of any information it contains.

A Facile Method to Enhance Ferroelectric Properties in PVDF Nanocomposites

Mohammad Mahdi Abolhasani^{1a}, Fatemeh Zarejousheghani^a, Zhenxiang Cheng^b, Minoos Naebe^c

^aChemical Engineering Department, University of Kashan, Kashan, Iran

^bInstitute for Superconducting & Electronic Materials, University of Wollongong, NSW 2500, Australia

^cInstitute for Frontier Materials, Deakin University, VIC 3216, Australia

Abstract

Poly(vinylidene fluoride) (PVDF)/nanoclay composites were prepared using melt compounding. Effect of acrylic rubber (ACM) as a compatibilizer on different polymorph formation and ferroelectric properties of nanocomposites were investigated. Intercalation and morphological structure of the samples were studied using X-ray diffraction (XRD) and transition electron microscopy (TEM). Infrared spectroscopy and X-ray analysis revealed the coexistence of β and γ crystalline forms in PVDF/Clay nanocomposite while in partially miscible PVDF/ACM/Clay hybrids three polymorphs of α , β and γ coexisted. Coefficients of Electric field-Polarization (E-P) Taylor expansion were calculated based on Lorentz theory. Using genetic algorithm, complex dielectric susceptibilities as well as dielectric constant for each sample were calculated and optimized. Predicted dielectric constant was found to be in quite good agreement with experimental results. A dielectric constant of 16 (10 Hz) was obtained for PVDF/ACM/Clay(90/10/5) which was 40% higher than that of PVDF/Clay(100/5) nanocomposite without ACM. The improved dielectric performance of the nanocomposites can be attributed to the compatibilizing effect of ACM which facilitated the growth of β polymorph in the sample.

Keywords: nanocomposite, polymorph, P-E hysteresis loop, dielectric constant, E-P Taylor expansion, modeling

¹ To whom correspondence should be addressed, E-mail: abolhasani@kashanu.ac.ir

Introduction

In last decade, ferroelectric materials have received numerous attentions due to their industrial applications, such as nonvolatile memory and transducers in sensors and actuators, electrostriction, electric energy storage, electrocaloric cooling, fuel injectors for high efficiency-low emission diesel engines, and ultrasonic rotary inchworm motors with high power and torque densities¹⁻⁵.

Ferroelectric materials are mainly divided into two groups: ceramics and polymer ferroelectrics. Ceramic ferroelectrics properties are highly desirable; however, they are brittle and quite heavy. On the other hand, the ferroelectric polymers are light, flexible, easy to process and low cost, nevertheless, their polar properties are an order of magnitude weaker^{1,6}. Among polymers, PVDF and its copolymers are the most well-known and widely used family of polymer ferroelectrics with significant ferroelectric properties mainly due to its β polymorph.

PVDF as a polymorphous crystallizable polymer has at least five crystal polymorphs, i.e., α , β , γ , ϵ and δ . However, only the β and γ crystalline phases with trans conformation have dipole moment in crystalline phase. So, the β and γ crystalline phases are the most important and attractive phases among others with outstanding electric properties⁷⁻¹⁰. Nevertheless, in study of polarizability, β polymorph plays a more significant role therefore many efforts have been made to induce formation of this polymorph type to take the full advantage of ferroelectric properties that PVDF has to offer.

Various methods have been proposed and implemented¹¹⁻¹⁴ to increase the β phase content of PVDF films; however high temperature mechanical stretching and high voltage poling are proved to be efficient and practical¹⁵⁻¹⁷.

Nanoparticles have been long used in polymer matrices to improve mechanical, thermal and electrical properties. The performance of polymer based nanocomposites depends on distribution and dispersion of nanoparticles within the matrix as well as the strength of the interfacial bonding between nanoparticles and polymer matrix¹⁸. It has been shown that employing block or graft copolymers as compatibilizing agents in nanocomposites can improve the interaction between polymer matrix and inorganic nanoparticles¹⁹.

Carbon-based nanoparticles have shown to enhance the ferroelectric and dielectric properties of polymers. Kim et al.¹⁷ have used multiwalled carbon nanotubes (MWCNTs) to improve piezo- and ferroelectric properties of PVDF matrix. Shang et al.²⁰ have used layered graphene nanosheets in PVDF polymer matrix and reported a high dielectric constant of 63 (100 Hz) upon addition of 1.27 vol% of graphene which was 9 times higher than that of pure PVDF. Yu et al.²¹ also studied graphene based nanocomposites and found that with a percolation threshold of 4.5 wt% a dielectric constant of 40 (100 Hz) was obtained. Ma et al.²² have studied the crystalline structure of polymer blends and revealed that PMMA can increase β phase content of PVDF, while Li et al.²³ have further investigated PVDF/PMMA ferroelectric properties and reported $4 \mu\text{C}/\text{m}^2$ of P_r for blend of PVDF with 20wt% PMMA. Moussaif et al.²⁴ reported that a small amount of PMMA can act as a compatibilizer and enhances the affinity of PVDF to organosilicate particles. However, in this study, no results are provided for the effect of PMMA on the crystalline structure of PVDF matrix.

Lately, it has been reported that addition of clay platelets into PVDF polymer matrix induces polar crystalline phase^{12,25-30}. Priya and Jog²⁵⁻²⁷ reported the effectiveness of organically modified montmorillonite for the induction of β polymorph formation in PVDF films. Peng et al.³¹ reported the nucleation of β polymorph with the addition of 1-2wt% clay, however, the nanocomposite containing 5wt% nanoclay exhibited reduced crystallinity. Shukla et al.³² have shown changes in dielectric constant as a result of frequency changes at room temperature for pure PVDF and PVDF nanocomposite containing 10wt% clay. At low frequency, dielectric constant of PVDF-clay nanocomposite were lower than pure PVDF, however, at 100 Hz this trend was reverse.

In the present study we have used inorganic nanofiller (clay) and a rubbery polymer (ACM) as a compatibilizer to prepare ferroelectric PVDF films. We have shown that the enhanced ferroelectric property can be obtained in a simple fashion and with no further post treatments such as high temperature stretching. A correlation was found between the improved ferroelectric properties and growth of β phase content in PVDF nanocomposites containing ACM compatibilizer. To the best of our knowledge it is the first time that the effect of intercalation of layered inorganic nano-fillers on ferroelectric properties of PVDF is studied.

To investigate the ferroelectric properties of PVDF/clay nanocomposites first the P-E hysteresis loops of nanocomposites which are indicative of polarizability were compared. The E-P Taylor expansion was then modeled using Lorentz theory. Finally, using the new generated equation, linear susceptibility or dielectric constant as well as nonlinear optical values were calculated.

Theory of ferroelectricity

There are two main theories to study the ferroelectric property of materials i.e. Landau-Devonshire theory³³ and Landau-Khalatnikov theory³⁴. Landau-Khalatnikov theory is a dynamical version of Landau-Devonshire by which P-E hysteresis loop could be regenerated.

According to Landau-Devonshire theory, Free energy, G, could be determined based on a few variables including temperature (T), electric field (E), polarization (P), stress (s), strain (e) and so forth.

In the absence of mechanical stress, free energy would be described as:

$$G = f(P_x, P_y, P_z, E, T) \quad \text{Equation 1}$$

where P_x , P_y , P_z are the components of the polarization, T is the temperature and E is the external electric field.

Assuming that for an uniaxial ferroelectric the free energy of unpolarized crystals is equal to zero³⁵⁻³⁷, the free energy, G, of polarized crystals could be written as:

$$G = \frac{1}{2} \alpha P^2 + \frac{1}{4} \gamma P^4 + \frac{1}{6} \delta P^6 + \dots - EP \quad \text{Equation 2}$$

For all known ferroelectrics, the coefficient α is a function of temperature; note that at below Curie temperature this coefficient is negative. The δ parameter is positive while γ depends on the type of transition (it is negative for first-order transitions and positive for second-order transitions).

In equilibrium thermodynamic condition at constant temperature, when $\left(\frac{\partial G}{\partial P}\right)_T = 0$, equation 2 can be rewritten as:

$$E = \alpha P + \gamma P^3 + \delta P^5 + \dots \quad \text{Equation 3}$$

Furthermore for uniaxial ferroelectric, general relation between polarization, P, and applied electric field, E, has been given as a Taylor expansion³⁸⁻⁴¹, namely:

$$P = a_1 E + a_2 E^2 + a_3 E^3 + \dots \quad \text{Equation 4}$$

where a_1 , a_2 & a_3 are the first, second, and third derivatives of Taylor expansion. In equation 4, $a_1 = \epsilon_0 \chi$, where χ or $\chi^{(1)}$ is the linear susceptibility and dimensionless physical property; $a_2 = \epsilon_0 \chi^{(2)}$ and $a_3 = \epsilon_0 \chi^{(3)}$ where $\chi^{(2)}$ & $\chi^{(3)}$ are first and second hyper-susceptibilities (sometimes referred to optical susceptibilities)³⁹. In general, the complex dielectric susceptibilities, $\chi^{(n)}$, are related to the microscopic (electronic and nuclear) structure of material³⁸ and are a function of the frequency of the applied electric field. Linear dielectric susceptibility is generally much larger than nonlinear coefficients $\chi^{(2)}$, $\chi^{(3)}$ and so forth. For dielectric crystals, semiconductors, and organic materials used in photonics application, $\chi^{(2)}$ are in the range of $10^{-13} - 10^{-10}(\text{m/V})$; and for glasses, crystals, semiconductors, semiconductor-doped glasses, and organic materials interested in photonics $\chi^{(3)}$ are in the vicinity of $10^{-23} - 10^{-16}(\text{Cm}^2/\text{V}^2)$.⁴⁰

The Lorentz classical theory is based on the classical theory of interaction between light and matter and is used to describe frequency dependent polarization due to bound charge. The bindings between electrons and nucleus are supposed to be similar to the that of a mass-spring system.⁴² The linear susceptibility $\chi(\omega)$ deduce from Lorentz theory:

$$\chi(\omega) = \frac{\omega_p^2}{\omega_0^2 - \omega^2 + i\Gamma\omega} \quad \text{Equation 5}$$

where ω_p is plasma frequency, ω_0 is resonant frequency and Γ is the damping factor. Based on equation 5, we can represent real and imaginary part of dielectric constant ($\epsilon_r = \epsilon' - j\epsilon''$) as:

$$\epsilon' = \frac{\omega_p^2(\omega_0^2 - \omega^2)}{(\omega_0^2 - \omega^2)^2 + \Gamma^2\omega^2} \quad \text{Equation 6}$$

$$\epsilon'' = \frac{\omega_p^2\Gamma\omega}{(\omega_0^2 - \omega^2)^2 + \Gamma^2\omega^2} \quad \text{Equation 7}$$

Experiments

Materials and methods

PVDF (Kynar 710) with melting flow rate of 25 g/10 min (2328C/12.5 kg load) from Arkema and acrylic rubber (Grade AR71) from Zeon Advanced Polymix Co.(Thailand) were used in this work. The major component of the acrylic rubber was poly (ethyl acrylate) (PEA), which contains a minor amount (5%w) of chlorine cure-site monomer. Organically modified clay, Cloisite 30B with a cation exchange capacity of 90 meq/100 g was supplied by Southern Clay. All components were dried in a vacuum oven at 80°C for at least 12h before processing. Clay content in composite samples is 5 wt%. From now on in this manuscript we use NPVDF, NACM, NPVDF/5ACM and NPVDF/10ACM nomenclature for PVDF nanocomposite, ACM nanocomposite and PVDF nanocomposite with 5% and 10% ACM as compatibilizer, respectively. All samples were prepared using a Brabender internal mixer at a rotation speed of 100rpm at 190°C for 10min. Samples were hot pressed at 200°C to a thin film and allowed to slowly cool down to room temperature.

Characterization

To investigate the level of clay layers dispersion, Molau test was done by adding 1 gram of PVDF/clay samples in 10 ml N,N-dimethylformamide (DMF). The mixture was shaken vigorously at 50°C and then left at room temperature for one month to observe the turbidity of the solutions.

Fourier transform infrared spectroscopy (FTIR) was carried out using Bruker 70 equipped with ATR unit. FTIR spectra were acquired (64 scans at 4 cm⁻¹ resolution) from 500 Cm⁻¹ to 1500 Cm⁻¹.

X-ray diffraction measurement was performed on a Panalytical XRD instrument. The data were recorded in the range of $2\theta = 2-10^\circ$. Samples were scanned continuously with a 0.5° scan step and 1 s scan time.

The composite samples were sectioned using a Leica UC6 ultramicrotome with FC6 cryochamber at -120°C, at a nominal thickness of 70 to 80 nm. Sections were imaged using a Gatan Orius SC1000 digital camera on a JEOL 2100 transmission electron microscope (TEM) operating at an accelerating voltage of 200kV.

Ferroelectric hysteresis loops were measured at ambient temperature with a continuous triangular wave signal electric field at frequency in the range of 5 to 100 Hz and amplitude up to 30 MV/m. Electric

polarization versus electric field was obtained using an Easy Check 300 (aixACCT Systems GmbH, Germany) equipped with Trek 610E high voltage amplifier T source for measurements at room temperature.

Results and discussion

FTIR analysis

In our earlier work, we showed⁴³⁻⁴⁸ that the neat PVDF and PVDF/ACM blends formed α polymorph, while PVDF/Clay nanocomposite induce both β and γ polymorphs. In this work our aim is to explore the compatibilizing effect of ACM on the ferroelectric polymorph formation of PVDF in the presence of nanoclay. figure (1.a) displays the FTIR spectra of neat PVDF, NPVDF, NPVDF/5ACM and NPVDF/10ACM samples. The frequencies and the vibrational assignments for α , β and γ phases are 763, 811 and 839 cm^{-1} , respectively⁴⁴. Neat PVDF shows only α phase characteristic peak while NPVDF sample showed both β and γ phase peak. However, for NPVDF/ACM sample all three polymorphs peaks are observable. This observation demonstrates that the presence of nanoclay hindered the formation of α polymorph in NPVDF sample while compatibilizing effect of ACM induced α phase formation. Formation of β and γ polymorph in NPVDF composite can be attributed to the similar crystal lattices between clay and these polymorphs²⁵, the presence of an ion-dipole interaction between nanoclay layers and PVDF chains in molten state¹² or different velocity regimes present in the nanocomposite⁴⁷.

To further explain the results, the change of α , β and γ phase contents for NPVDF, NPVDF/5ACM and NPVDF/10ACM samples are compared in table 1. The peak at 1072 cm^{-1} is selected as a reference band, because this band is well-known to be proportional only to the sample thickness regardless of the crystalline modification of PVDF⁴⁶. The ratio of FTIR absorbance of 763 cm^{-1} (α polymorph), 839 cm^{-1} (β polymorph) and 811 cm^{-1} (γ polymorph) with respect to the reference band are used to calculate the percent of α , β and γ polymorph as shown in table 1. Since the absorption peak at 1234 cm^{-1} is solely for γ polymorph, it can be employed for quantitative analysis. However, when this peak is detected as a shoulder, the content of γ polymorph cannot be calculated quantitatively as it is difficult to separate this peak from the overlapped peaks of the two other crystalline polymorphs, i.e. α and β , at 1214 and 1276 cm^{-1} , respectively. Therefore, the very small but discernible shoulder at 811 cm^{-1} is designated to

show the change in the γ polymorph content in the resultant samples. As seen in table 1. Addition of ACM as a compatibilizer has increased the β phase content from 17% in NPVDF to 21% and 30% in NPVDF/5ACM and NPVDF/10ACM samples, respectively. High amount of γ phase in NPVDF is related to the molecular chains which have had enough time to form gauche defect at high temperatures or crystallization within rose regime⁴⁷. However, decreasing the γ phase content and increasing the β polymorph by addition of compatibilizer can be related to better dispersion of clay in presence of ACM which can result in enhanced nucleation of β polymorph in NPVDF/5ACM and NPVDF/10ACM samples compared to NPVDF nanocomposite. In other words, in NPVDF/ACM sample nucleation of β polymorph is facilitated. Meanwhile, nucleation of α phase is related to the nucleus which formed independent of nanoclays due to hindrance effect of ACM. We have recently reported this phenomenon for PVDF/ACM/Clay hybrid with more than 70%wt ACM content^{37, 42}. Note that in this work all composite samples were hot pressed and slowly cooled down to room temperature when increasing the β phase content was simply achieved by addition of a compatibilizer. Obtaining even larger β phase content is possible by isothermal crystallization and stretching at high temperature which is the subject of our next paper. In the following section we will show that the increase in the electroactive β polymorph leads to improved ferroelectric properties of NPVDF/5ACM and NPVDF/5ACM samples compared to NPVDF nanocomposites. However, pure PVDF showed solely α polymorph therefore its ferroelectric properties was not investigated in this study.

Morphology and clay dispersion

Figure (1.b) presents the WAXD patterns of Cloisite 30B, NPVDF, NACM, NPVDF/5ACM and NPVDF/10ACM samples. The Cloisite 30B has a d-spacing of 1.8nm, evidenced by the XRD peak at $2\theta \sim 4.8^\circ$. In the NPVDF containing 5 wt% clay, this peak is shifted towards the left (lower frequencies), resulting in a diffused peak at $2\theta \sim 2.5^\circ$, corresponding to d-spacing of 3.4nm. This suggests that the PVDF has penetrated into the gallery region and formed the intercalated structure with increase in the clay interlayer space. This type of structure is formed due to the interaction between the modified clay and PVDF or shear induced intercalation. The peak at $2\theta \sim 5.8^\circ$ corresponding to the d-spacing 1.4nm is due to the second order diffraction $d(002)$ ⁴⁵. The appearance of this peak could be attributed to a partially

collapsed structure resulting from quaternary ammonium degradation. NACM, NPVDF/5ACM and NPVDF/10ACM samples showed different behavior, these samples has two small peaks at $2\theta \sim 2^\circ$ corresponding to d-spacing of 4.2nm and a broad peak at around $2\theta \sim 5^\circ$ which is almost the same as the neat Cloisite 30B peak. However, the relative intensity of the peak reduced significantly which suggests that the clay is exfoliated but a small fraction of the clay layers remain as local aggregates in ACM nanocomposites.

TEM images for NPVDF, NACM, NPVDF/5ACM and NPVDF/10ACM samples are shown in figure (2). TEM images of NPVDF shows clearly the clay tactoids which have a thickness of ~ 150 nm as a result of high interfacial tension between PVDF and Cloisite 30B. From TEM images it can be seen that NPVDF sample failed to form an exfoliated structure. In sharp contrast, NACM, NPVDF/5ACM and NPVDF/10ACM samples showed individual layers as well as stacks containing parallel oriented layers with various degree of intercalation. The compatibilizing effect of ACM chains is enhanced by the strong polar interaction developed between the oxygen groups of the silicate and the oxygen groups of ACM. Therefore ACM acts as a compatibilizer and increases the intercalation of nanoclay in PVDF.

Effects of ACM on ferroelectric & dielectric properties of NPVDF nanocomposite

P-E hysteresis loop & dielectric

As earlier discussed, a common method to observe ferroelectric polarization characteristic is via the hysteresis loop which can be translated into the existence of β phase crystals in PVDF polymer. Figures 3, shows the sequence of polarization for applied electric at 20 MV/m in different frequencies for NPVDF, NPVDF/5ACM and NPVDF/10ACM nanocomposites, respectively.

In all samples, rise in frequencies is resulted in decreasing polarization this suggests that the increase in time of applied electric field induced more polarized dipole moment.

Comparing NPVDF, NPVDF/5ACM and NPVDF/10ACM composites revealed that ACM has increased the polarization up to 100-fold at the same frequency and electric field. This observation is associated to the crystal structure of PVDF, in which β polymorph nucleation increased in the presence of ACM. Addition of ACM would also affect the number of domains, a region of a ferroelectric material within which the spontaneous polarization is constant.

For all samples, the polarization increased with decreasing the frequency from 100 to 5Hz, however this increase is more pronounced at higher frequencies. This phenomenon is independent of electric field which confirms that change in electric field at constant frequency won't change the polarization mechanism; however it would increase polarizability.

Note that decrease in frequency increased the area under the curve which is associated to the dissipated energy. Therefore, optimization of dielectric constant and dissipated energy has been an interesting subject of research for many years^{1,49}.

For determination of polarization mechanism, in figure 4 real and imaginary part of dielectric constant are shown at evaluated temperature for NPVDF, NPVDF/5ACM and NPVDF/10ACM nanocomposites, respectively.

For all samples, according to real part of dielectric constant, orientational (dipolar) and atomic polarization are seen below hundred Hz & at 1 MHz, respectively. With increase in the amount of dielectric constant and based on ACM effect, increase in nucleation rise the reflex of dipolar polarization 40% faster than samples without it, also decrease the loss dielectric.

Figures 5, 6 and 7 are shown temperature gradient of dielectric constant for all samples. With comparison increase dielectric constant respect to temperature for all samples, ACM shift Curie temperature to higher amount.

Calculation of dielectric & nonlinear optical constants

To calculate the dielectric constant as well as optical susceptibilities of nanocomposites (represented by equation 4), the Lorentz theory is used.

In the second step, using genetic algorithm and a series of data, equation 4 in combination with equations 5-7 is optimized. Objective function, OF, are defined as:

$$OF = \sum(P - (a_1E + a_2E^2 + a_3E^3))^2 \quad \text{Equation 8}$$

The results of optimization for NPVDF, NPVDF/5ACM and NPVDF/10ACM nanocomposites were calculated using P-E hysteresis data and are reported in Table 2. As it can be seen, the addition of ACM as a compatibilizer in nanocomposite has increased the dielectric constant of NPVDF/5ACM nanocomposite up to 30% compared to NPVDF and up to 33% for NPVDF/10ACM compared to NPVDF/5ACM. Note

that this increase in dielectric constant was obtained simply by addition of ACM into PVDF nanocomposite. However, we believe that further increase in ferroelectric constant can be achieved using optimum amount of clay, ACM, isothermal crystallization and high temperature stretching of samples.

As mentioned above, dependency of polarization to frequency varies from 100 to 5 Hz. This observation may be attributed to the ionic polarization or decrease in dissipation factor which arises in low frequencies i.e. 10 Hz⁴⁹. It is worth to mention that PVDF nanocomposites containing ACM compatibilizer showed larger optical susceptibilities compared to well-known commercial PVDF films (Table 2). Finally, the dielectric susceptibilities obtained by using genetic algorithm optimization applied to the equation 4.

Results (Table 2) are compared with experimental data (Figure 4). This shows a good agreement between theoretical and experimental data, using genetic algorithm along with information on P-E hysteresis data.

Conclusion

In this study, compatibilizing effect of ACM on various polymorph contents of PVDF was investigated. WAXD and TEM results proved that clay tactoids formed an intercalated structure in PVDF nanocomposite while ACM compatibilized nanocomposites showed individual layers as well as stacks containing parallel and oriented layers with various degree of intercalation. FTIR analysis revealed the formation of β and γ polymorphs in NPVDF nanocomposite and α , β and γ polymorphs in both NPVDF/5ACM and NPVDF/10ACM samples. Investigation of ferroelectric properties of nanocomposites containing 5 and 10%wt ACM showed 89% and 98% increase in polarization and 30% and 70% improvement in dielectric constant, respectively, compared to samples without ACM. This is due to the enlargement of β polymorph in the presence of ACM. Theoretical value of polarization calculated using optimized coefficient was found to be in good agreement with experimental results. A dielectric constant of 16 (100 Hz) was obtained for PVDF/10ACM/Clay which was 40% higher than that of PVDF/Clay nanocomposite. It is expected that employing the mechanical and thermal processes such as isothermal crystallization and high temperature drawing of nanocomposites combined with optimum amount of clay and ACM can significantly improve the ferroelectric properties of PVDF. This is the subject of our current research and will be reported in future.

Reference

- (1) Yang, L.; Li, X.; Allahyarov, E.; Taylor, P. L.; Zhang, Q. M.; Zhu, L. *Polymer* **2013**, *54*, 1709.
- (2) Scott, J. F. *Science* **2007**, *315*, 954.
- (3) Landis, C. M. *Current Opinion in Solid State and Materials Science* **2004**, *8*, 59.
- (4) Muralt, P. *Journal of Micromechanics and Microengineering* **2000**, *10*, 136.
- (5) Asadi, K.; de Leeuw, D. M.; de Boer, B.; Blom, P. W. M. *Nat Mater* **2008**, *7*, 547.
- (6) Bernholc, J.; Nakhmanson, S. M.; Nardelli, M. B.; Meunier, V. *Computing in Science & Engineering* **2004**, *6*, 12.
- (7) Yang, J.; Wang, J.; Zhang, Q.; Chen, F.; Deng, H.; Wang, K.; Fu, Q. *Polymer* **2011**, *52*, 4970.
- (8) Guerra, G.; Karasz, F. E.; MacKnight, W. J. *Macromolecules* **1986**, *19*, 1935.
- (9) Hattori, T.; Hikosaka, M.; Ohigashi, H. *Polymer* **1996**, *37*, 85.
- (10) Gregorio Jr, R.; Borges, D. S. *Polymer* **2008**, *49*, 4009.
- (11) He, X.; Yao, K. *Applied Physics Letters* **2006**, *89*.
- (12) Shah, D.; Maiti, P.; Gunn, E.; Schmidt, D. F.; Jiang, D. D.; Batt, C. A.; Giannelis, E. P. *Advanced Materials* **2004**, *16*, 1173.
- (13) Benz, M.; Euler, W. B. *Journal of Applied Polymer Science* **2003**, *89*, 1093.
- (14) Yu, S.; Zheng, W.; Yu, W.; Zhang, Y.; Jiang, Q.; Zhao, Z. *Macromolecules* **2009**, *42*, 8870.
- (15) Du, C.-h.; Zhu, B.-K.; Xu, Y.-Y. *Journal of Applied Polymer Science* **2007**, *104*, 2254.
- (16) Sajkiewicz, P.; Wasiak, A.; Goclowski, Z. *European Polymer Journal* **1999**, *35*, 423.
- (17) Kim, G. H.; Hong, S. M.; Seo, Y. *Phys Chem Chem Phys* **2009**, *11*, 10506.
- (18) Naebe, M.; Wang, J.; Amini, A.; Khayyam, H.; Hameed, N.; Li, L. H.; Chen, Y.; Fox, B. *Scientific reports* **2014**, *4*.
- (19) Giannelis, E. P. *Advanced Materials* **1996**, *8*, 29.
- (20) Shang, J.; Zhang, Y.; Yu, L.; Shen, B.; Lv, F.; Chu, P. K. *Materials Chemistry and Physics* **2012**, *134*, 867.
- (21) Jinhong, Y.; Xingyi, H.; Chao, W.; Pingkai, J. *Dielectrics and Electrical Insulation, IEEE Transactions on* **2011**, *18*, 478.
- (22) Ma, W.; Zhang, J.; Wang, X.; Wang, S. *Applied Surface Science* **2007**, *253*, 8377.
- (23) Li, M.; Stingelin, N.; Michels, J. J.; Spijkman, M.-J.; Asadi, K.; Feldman, K.; Blom, P. W. M.; de Leeuw, D. M. *Macromolecules* **2012**, *45*, 7477.
- (24) Moussaif, N.; Groeninckx, G. *Polymer* **2003**, *44*, 7899.
- (25) Priya, L.; Jog, J. P. *Journal of Polymer Science Part B: Polymer Physics* **2002**, *40*, 1682.
- (26) Priya, L.; Jog, J. P. *Journal of Applied Polymer Science* **2003**, *89*, 2036.
- (27) Priya, L.; Jog, J. P. *Journal of Polymer Science Part B: Polymer Physics* **2003**, *41*, 31.
- (28) Asai, K.; Okamoto, M.; Tashiro, K. *Polymer* **2008**, *49*, 4298.
- (29) Asai, K.; Okamoto, M.; Tashiro, K. *Polymer* **2008**, *49*, 5186.
- (30) Buckley, J.; Cebe, P.; Cherdack, D.; Crawford, J.; Ince, B. S.; Jenkins, M.; Pan, J.; Reveley, M.; Washington, N.; Wolchover, N. *Polymer* **2006**, *47*, 2411.
- (31) Peng, Q.-Y.; Cong, P.-H.; Liu, X.-J.; Liu, T.-X.; Huang, S.; Li, T.-S. *Wear* **2009**, *266*, 713.
- (32) Shukla, N.; Shukla, A.; Thakur, A. K.; Choudhary, R. N. P. *Indian Journal of Engineering & Materials Sciences* **2008**, *15*, 7.
- (33) Chandra, P.; Littlewood, P. In *Physics of Ferroelectrics*; Springer Berlin Heidelberg: 2007; Vol. 105, p 69.
- (34) Lo, V. C. *Journal of Applied Physics* **2003**, *94*, 3353.
- (35) Dekker, A. J. *Solid state physics*; Prentice-Hall, 1965.
- (36) Kochervinskii, V. V. *Russian Chemical Reviews* **1999**, *68*, 821.
- (37) Safari, A.; Akdogan, E. K. *Piezoelectric and Acoustic Materials for Transducer Applications*; Springer, 2008.

- (38) Sinha, C.; Bhattacharyya, S. S. *Current Topics in Atomic, Molecular and Optical Physics: Invited Lectures Delivered at the Conference on Atomic Molecular and Optical Physics (TC 2005), 13th-15th December, 2005, Indian Association for the Cultivation of Science, Kolkata, India*; World Scientific, 2007.
- (39) Cardarelli, F. *Materials Handbook: A Concise Desktop Reference*; Springer, 2008.
- (40) Bloembergen, N. *Nonlinear Optics*; World Scientific, 1996.
- (41) Van Stryland, E. W.; Williams, D. R.; Wolfe, W. L.; Optical Society of America, W., DC. *Handbook of Optics. Vol. 2. Devices, Measurements, Andproperties*; McGraw-Hill, Incorporated, 1995.
- (42) Etchegoin, P. G.; Le Ru, E. C.; Meyer, M. *The Journal of Chemical Physics* **2006**, *125*.
- (43) Abolhasani, M. M.; Jalali-Arani, A.; Nazockdast, H.; Guo, Q. *Polymer* **2013**, *54*, 4686.
- (44) Abolhasani, M. M.; Guo, Q.; Jalali-Arani, A.; Nazockdast, H. *Journal of Applied Polymer Science* **2013**, *130*, 1247.
- (45) Abolhasani, M. M.; Naebe, M.; Jalali-Arani, A.; Guo, Q. *Nano* **2014**, *09*, 1450065.
- (46) Abolhasani, M. M.; Naebe, M.; Guo, Q. *Physical Chemistry Chemical Physics* **2014**, *16*, 10679.
- (47) Abolhasani, M. M.; Rezaei-Abadchi, M.; Magniez, K.; Guo, Q. *Journal of Thermal Analysis and Calorimetry* **2015**, *119*, 527.
- (48) Abolhasani, M. M.; Naebe, M.; Jalali-Arani, A.; Guo, Q. *PloS one* **2014**, *9*, e88715.
- (49) Zhu, L.; Wang, Q. *Macromolecules* **2012**, *45*, 2937.

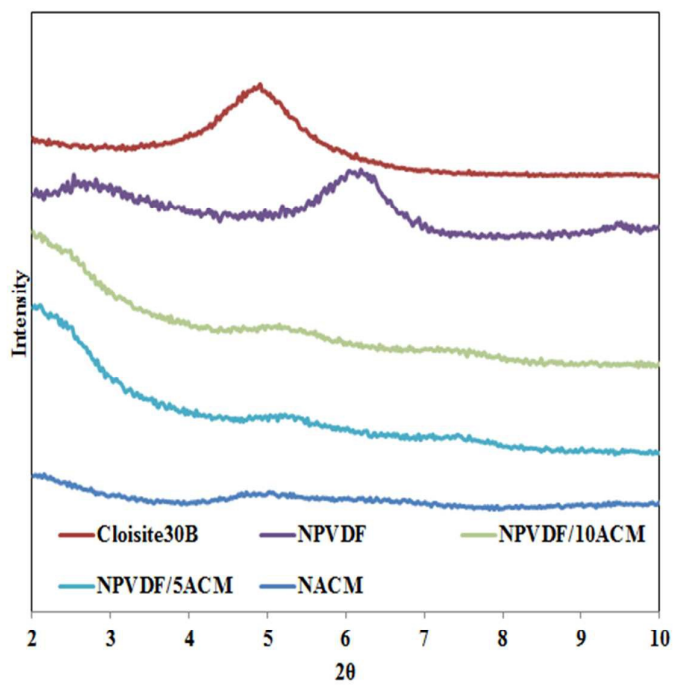
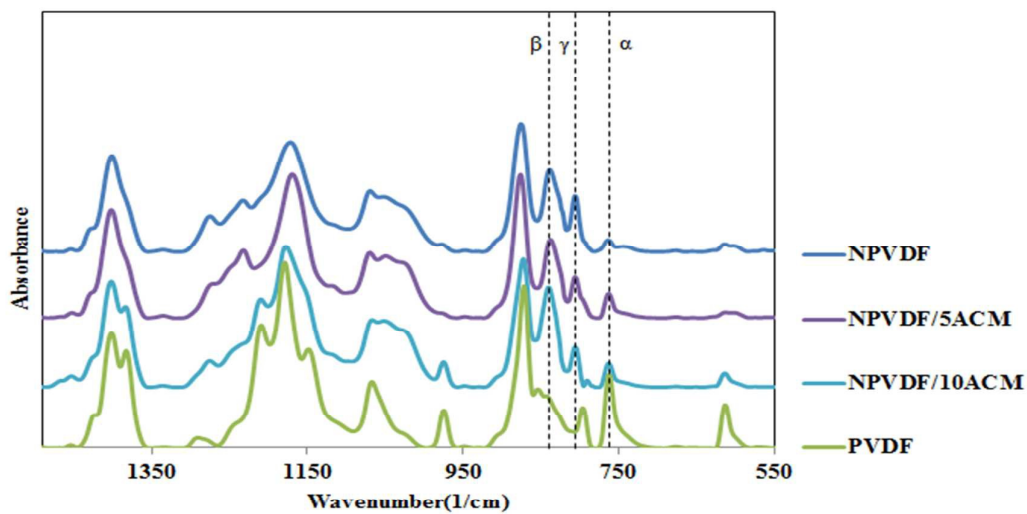


FIG 1. a) FTIR spectrum, b) WAXD profile of prepared samples.

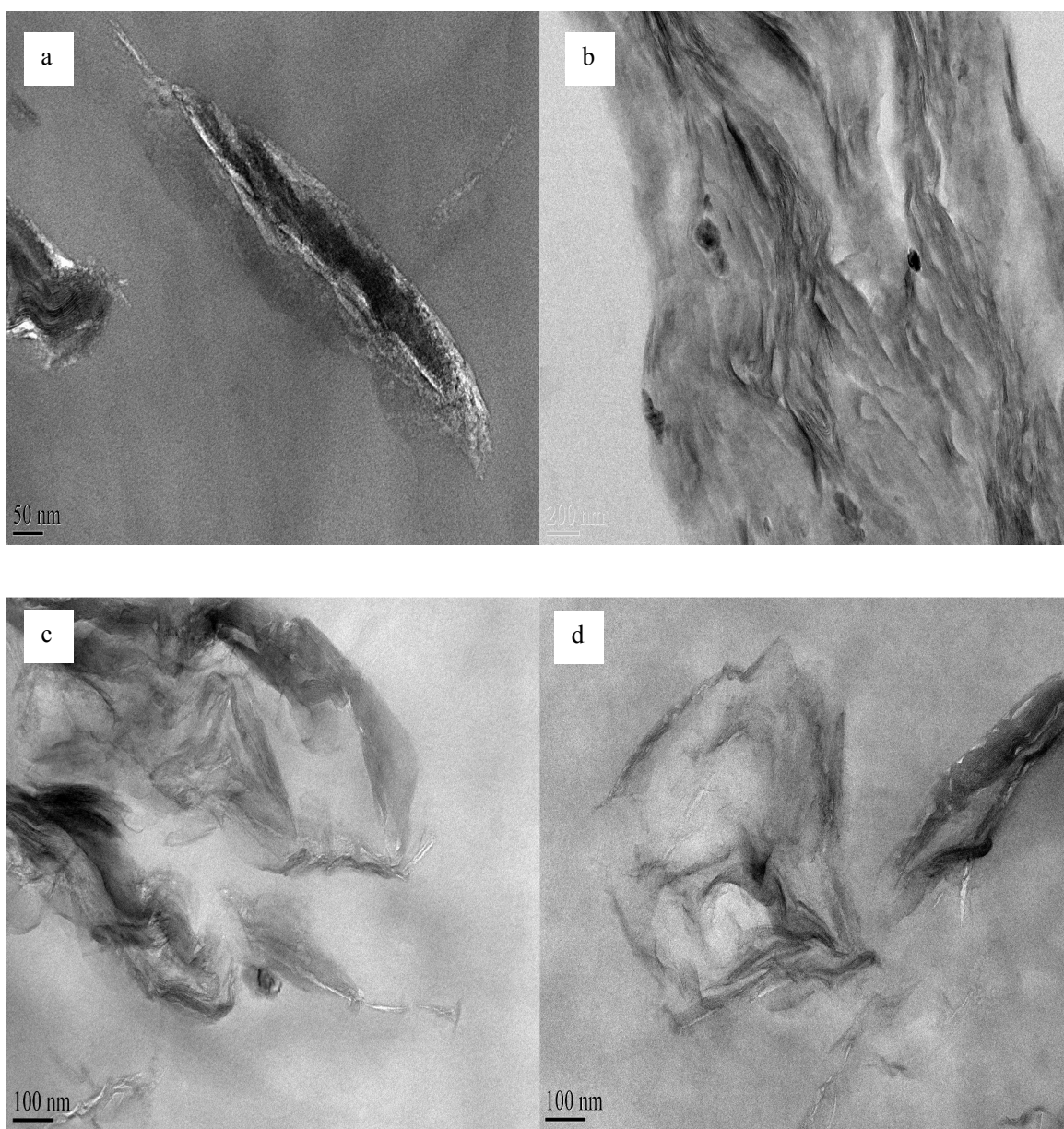


FIG. 2. TEM images of a) NPVDF, b)NACM, c) NPVDF/5ACM and d) NPVDF/10ACM.

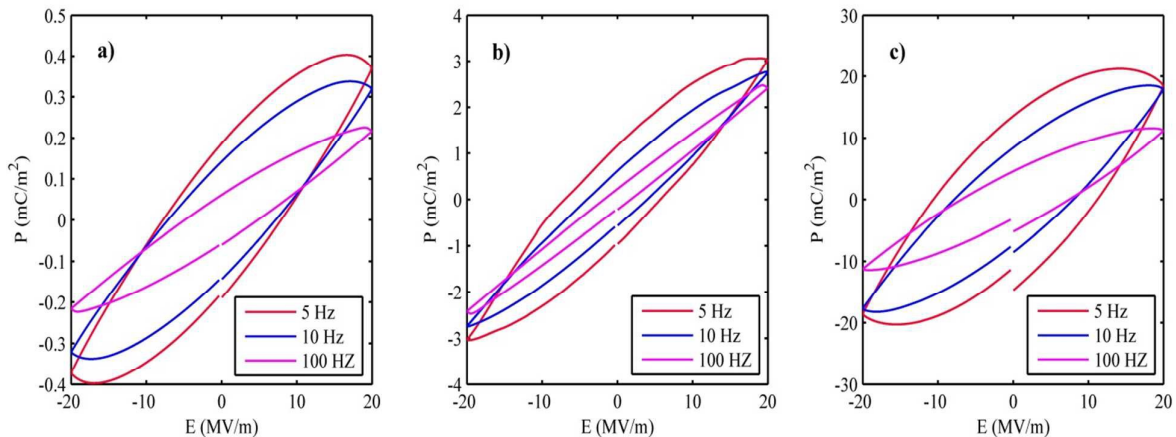


FIG 3. ((P-E hysteresis loops for a) NPVDF, b) NPVDF/5ACM and c) NPVDF/10ACM at evaluated temperature in different frequencies, 5 Hz, 10 Hz and 100 Hz.))

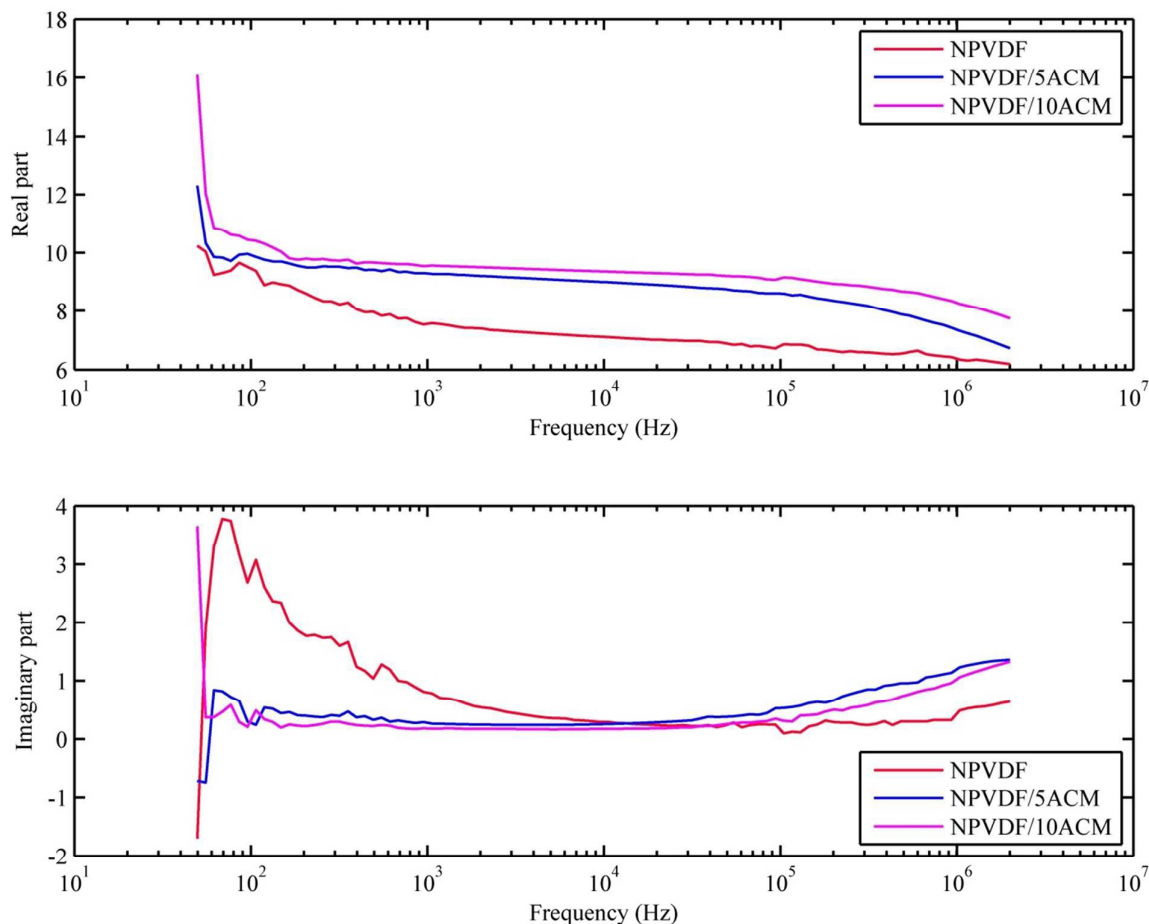


FIG 4. ((Frequency dependence for the real and imaginary components of the dielectric permittivity for NPVDF, NPVDF/5ACM and NPVDF/10ACM at evaluated.))

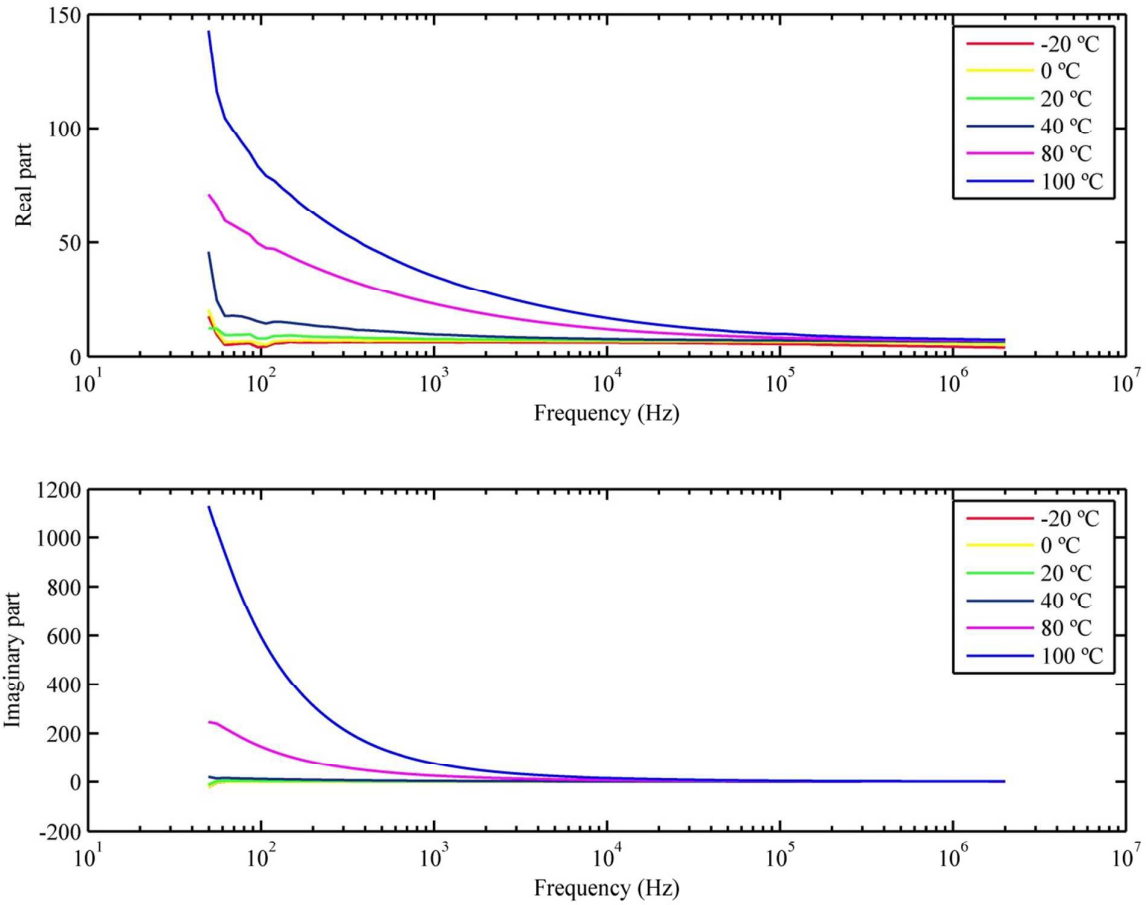


FIG 5. ((Frequency dependence for the real and imaginary components of the dielectric permittivity for NPVDF at different temperature.))

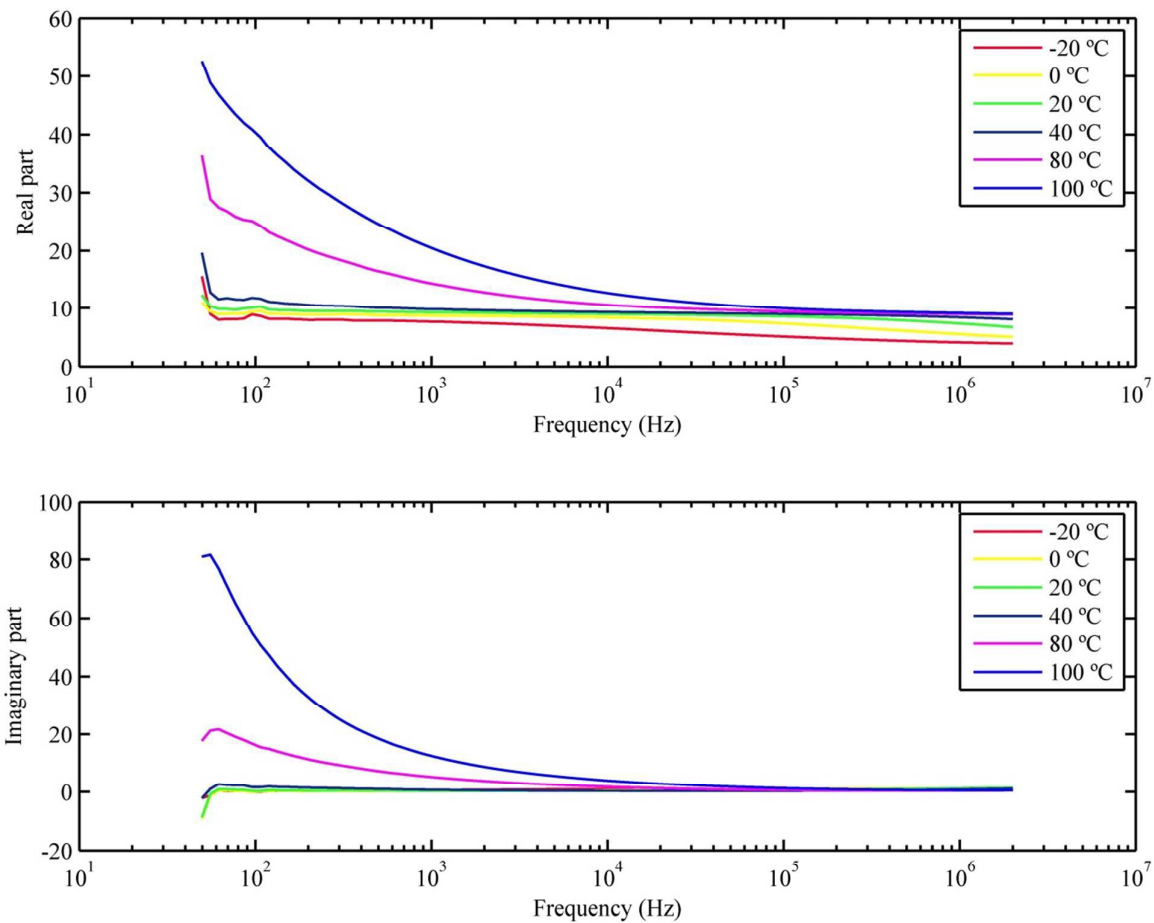


FIG 6. ((Frequency dependence for the real and imaginary components of the dielectric permittivity for NPVDF/5ACM at different temperature.))

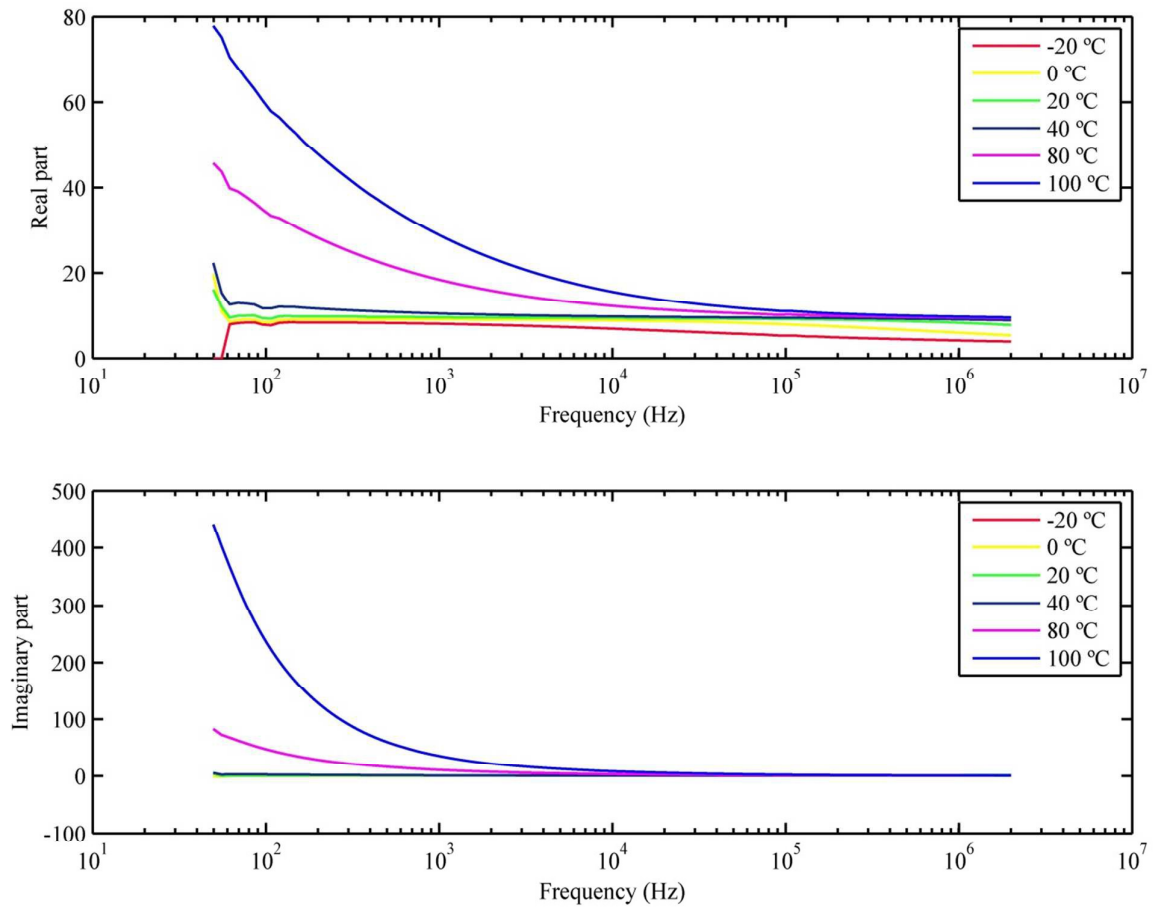


FIG 7. ((Frequency dependence for the real and imaginary components of the dielectric permittivity for NPVDF/10ACM at different temperature.))

Table 1. Quantitative analysis of percent of crystallinity and different polymorphs.

<i>Sample</i>	<i>Crystallinity</i>	α	β	γ
PVDF	51%	45%	4%	2%
NPVDF	46%	3%	15%	28%
NPVDF/5ACM	47%	6%	14%	21%
NPVDF/10ACM	46%	11%	30%	5%

Table 2. ((Dielectric constant and the complex dielectric susceptibilities, $\chi^{(n)}$, for NPVDF, NPVDF/5ACM and NPVDF/10ACM samples.))

Samples name	Frequency (Hz)	ϵ'	$\chi^{(2)}$ (m/V)	$\chi^{(3)}$ (Cm ² /V ²)
NPVDF	5	14.86	-1.650E-11	2.112E-18
NPVDF	10	13.15	-1.074E-11	1.046E-18
NPVDF	100	9.85	-5.580E-12	4.372E-19
NPVDF/5ACM	5	20.45	-3.596E-10	1.284E-17
NPVDF/5ACM	10	16.47	-2.549E-10	7.170E-18
NPVDF/5ACM	100	12.56	-8.206E-11	3.231E-18
NPVDF/10ACM	5	29.6	-1.627E-09	3.752E-17
NPVDF/10ACM	10	24.91	-1.402E-09	3.016E-17
NPVDF/10ACM	100	12.78	-5.305E-10	6.680E-18